# Evidence for a Nonendosomal Function of the *Saccharomyces cerevisiae* ESCRT-III-Like Protein Chm7

**Iva Bauer,* Thomas Brune,* Richard Preiss,† and Ralf Kölling*,[1]**

*Institut für Lebensmittelwissenschaft und Biotechnologie, Fg. Hefegenetik und Gärungstechnologie, Universität Hohenheim, 70599 Stuttgart, Germany, and †Department of Molecular and Cellular Biology, University of Guelph, Ontario, Canada N1G 2W1

**ABSTRACT** Endosomal sorting complex required for transport (ESCRT) proteins are involved in a number of cellular processes, such as endosomal protein sorting, HIV budding, cytokinesis, plasma membrane repair, and resealing of the nuclear envelope during mitosis. Here we explored the function of a noncanonical member of the ESCRT-III protein family, the *Saccharomyces cerevisiae* ortholog of human CHMP7. Very little is known about this protein. *In silico* analysis predicted that Chm7 (yeast ORF YJL049w) is a fusion of an ESCRT-II and ESCRT-III-like domain, which would suggest a role in endosomal protein sorting. However, our data argue against a role of Chm7 in endosomal protein sorting. The turnover of the endocytic cargo protein Ste6 and the vacuolar protein sorting of carboxypeptidase S (CPS) were not affected by *CHM7* deletion, and Chm7 also responded very differently to a loss in Vps4 function compared to a canonical ESCRT-III protein. Our data indicate that the Chm7 function could be connected to the endoplasmic reticulum (ER). In line with a function at the ER, we observed a strong negative genetic interaction between the deletion of a gene function (*APQ12*) implicated in nuclear pore complex assembly and messenger RNA (mRNA) export and the *CHM7* deletion. The patterns of genetic interactions between the *APQ12* deletion and deletions of ESCRT-III genes, two-hybrid interactions, and the specific localization of mCherry fusion proteins are consistent with the notion that Chm7 performs a novel function at the ER as part of an alternative ESCRT-III complex.

**KEYWORDS** ESCRT-III; multivesicular body; endosome; endoplasmic reticulum; protein degradation

THE endosomal sorting complex required for transport (ESCRT) system is very ancient. The basic components, an ESCRT-III-like protein and a protein homologous to the AAA-ATPase Vps4, were already present in the "last common eukaryotic ancestor" and are still found in all eukaryotic organisms to date (Leung *et al.* 2008). Furthermore, these components are even found in species of the crenarchaeal genus *Sulfolobus*, where they play a key role in cell division (Samson *et al.* 2008).

The ESCRT system was first identified in yeast by its role in endosomal protein sorting (Katzmann *et al.* 2001; Babst *et al.* 2002a,b). At present, this is the most thoroughly studied and best understood process involving ESCRT proteins. According to biochemical experiments, the ESCRT proteins can be grouped into several protein complexes called ESCRT-0, ESCRT-I, ESCRT-II, and ESCRT-III (Teis *et al.* 2008). It is thought that these protein complexes function consecutively in the recruitment and packaging of endocytic cargo proteins—bound for degradation in the lysosome or yeast vacuole—into vesicles that bud into the interior of the endosome. In the process of intraluminal vesicle (ILV) formation, ESCRT-III, in conjunction with Vps4, is involved in the abscission step, *i.e.*, release of the vesicle from the membrane into the interior of the endosome (Wollert *et al.* 2009).

In yeast, the classical ESCRT-III protein family consists of six small hydrophilic, mostly α-helical proteins (Howard *et al.* 2001; Kranz *et al.* 2001). There are counterparts to these six proteins in human cells that are called CHMPs (**ch**arged **m**ultivesicular body **p**roteins) (Howard *et al.* 2001). Gene duplications in some of the groups led to an expansion of the gene family. The proteins are (yeast/human) Did2/CHMP1A, CHMP1B; Did4 (Vps2)/CHMP2A, CHMP2B; Mos10 (Vps60)/CHMP5; Snf7 (Vps32)/CHMP4A, CHMP4B, CHMP4C; Vps20/CHMP6; and Vps24/CHMP3. In addition, there are two ESCRT-III-like proteins of larger size that contain


doi: 10.1534/genetics.115.178939
Manuscript received June 2, 2015; accepted for publication October 15, 2015; published Early Online October 26, 2015.
[1]Corresponding author: Institut für Lebensmittelwissenschaft und Biotechnologie, Fg. Hefegenetik und Gärungstechnologie (150f), Universität Hohenheim, Garbenstr. 23, 70599 Stuttgart, Germany. E-mail: ralf.koelling@uni-hohenheim.de

**Table 1 Yeast strains**

| Strain | Genotype[a] | Reference |
|---|---|---|
| JD52 | *MAT***a** *his3-Δ200 leu2-3,112 lys2-801 trp1-Δ63 ura3-52* | J. Dohmen, Köln |
| PJ69-4A | *MAT***a** *ade2 trp1-901 leu2-3,112 ura3-52 his3-Δ200 gal4Δ gal80Δ LYS2::(GAL1-HIS3 GAL2-ADE2) met2::GAL7-lacZ* | James *et al.* (1996) |
| RKY1509 | *Δmos10/Δvps60::kan*$^r$ | Kranz *et al.* (2001) |
| RKY1510 | *Δsnf7::HIS3* | Kranz *et al.* (2001) |
| RKY1511 | *Δvps4::HIS3* | Kranz *et al.* (2001) |
| RKY1590 | *Δvps20::HIS3* | Kranz *et al.* (2001) |
| RKY1728 | *Δdid2::HIS3* | Weiss *et al.* (2008) |
| RKY1730 | *Δvps24::HIS3* | Weiss *et al.* (2008) |
| RKY1732 | *Δdid4/Δvps2::HIS3* | Weiss *et al.* (2008) |
| RKY2302 | *CHM7-3HA::HIS3* | This study |
| RKY2468 | *Δchm7::kan*$^r$ | This study |
| RKY2495 | *CHM7-3HA::HIS3 Δvps4::TRP1* | This study |
| RKY2681 | *Δist1::HIS3* | This study |
| RKY2685 | *Δapq12::HIS3* | This study |
| RKY2686 | *NUP1-GFP::HIS3* | This study |
| RKY2687 | *NUP82-GFP::HIS3* | This study |
| RKY2686 | *Δchm7::kan*$^r$ *NUP1-GFP::HIS3* | This study |
| RKY2687 | *Δchm7::kan*$^r$ *NUP82-GFP::HIS3* | This study |
| RKY2693 | *Δapq12::HIS3 Δchm7::kan*$^r$ | This study |
| RKY2725 | *Δchm7::kan*$^r$ *SEC63-GFP::HIS3* | This study |
| RKY2755 | *Δvta1::HIS3* | This study |
| RKY2757 | *Δchm7::kan*$^r$ *Δist1::HIS3* | This study |
| RKY2759 | *Δapq12::kan*$^r$ *Δmos10::HIS3* | This study |
| RKY2760 | *Δapq12::kan*$^r$ *Δist1::HIS3* | This study |
| RKY2761 | *Δapq12::kan*$^r$ *Δvta1::HIS3* | This study |
| RKY2764 | *Δapq12::kan*$^r$ *Δdid2::HIS3* | This study |
| RKY2766 | *Δapq12::kan*$^r$ *Δvps24::HIS3* | This study |
| RKY2770 | *Δapq12::kan*$^r$ *Δsnf7::HIS3* | This study |
| RKY2773 | *Δapq12::kan*$^r$ *Δvps2::HIS3* | This study |
| RKY2775 | *Δapq12::kan*$^r$ *Δvps20::HIS3* | This study |

[a] RKY strains all based on JD52.

an ESCRT-III domain, Ist1/IST1 (Dimaano *et al.* 2008; Rue *et al.* 2008; Bajorek *et al.* 2009) and CHMP7 (Horii *et al.* 2006).

The protein complex biochemically defined as ESCRT-III consists of four subunits: Snf7, Vps2, Vps20, and Vps24 (Babst *et al.* 2002a). The exact composition of the complex is unclear. The main component of ESCRT-III seems to be Snf7 (Teis *et al.* 2008), which forms a circular filament surrounding the neck of the budding ILV (Henne *et al.* 2012). The current view is that Vps20 induces Snf7 filament formation by binding simultaneously to ESCRT-II and Snf7, while Vps2 and Vps24 limit the extent of filamentation and induce disassembly of the complex in conjunction with Did2, Vta1, and Vps4 (Nickerson *et al.* 2006; Saksena *et al.* 2009). The propensity to form filaments seems to be a general property of ESCRT-III proteins. So far, homo- or hetero-oligomeric filaments have been described for CHMP1B, CHMP2A, CHMP2B, Vps24 and CHMP3, Snf7 and CHMP4A, CHMP4B, and IST1 (Ghazi-Tabatabai *et al.* 2008; Hanson *et al.* 2008; Lata *et al.* 2008b; Bajorek *et al.* 2009; Bodon *et al.* 2011; Henne *et al.* 2012).

ESCRT-III proteins appear to be synthesized in an inactive "closed" conformation, preventing filament formation (Lata *et al.* 2008a; Bajorek *et al.* 2009). The three-dimensional structure has been solved for some ESCRT-III proteins (Muziol *et al.* 2006; Bajorek *et al.* 2009). The basic structure consists of six α-helices. The N-terminal core domain is made of a four-helical bundle, while the downstream helices mediate autoinhibition by folding back against the core domain (Bajorek *et al.* 2009). Autoinhibition appears to be released via interactions with the C-terminal region. Most ESCRT-III proteins contain short-sequence motifs in their C-terminal region that bind to MIT domains. Different motifs were identified (MIM1–5) (Skalicky *et al.* 2012) that bind to different surfaces on the MIT domain of MIT domain–containing proteins such as Vps4 and Vta1 (Obita *et al.* 2007; Stuchell-Brereton *et al.* 2007; Kieffer *et al.* 2008). Vps4 binding to the MIT-interacting motifs (MIMs) could induce disassembly of the ESCRT-III complex, or it could be involved in relieving autoinhibition of ESCRT-III proteins (Bodon *et al.* 2011).

Here we focus on the yeast counterpart of the human ESCRT-III-like protein CHMP7. CHMP7 is twice the size of a normal ESCRT-III protein and contains an ESCRT-III domain in its C-terminal half. Very little was known about this protein until very recently. In the initial publication (Horii *et al.* 2006), it was concluded that CHMP7 functions in the endosomal sorting pathway. Now evidence has been presented that an ESCRT-III complex containing CHMP7 as a subunit is involved in resealing of the nuclear envelope during mitosis (Olmos *et al.* 2015; Vietri *et al.* 2015). Earlier work also pointed to a role of CHMP7 in mitosis (Morita *et al.* 2010). In another report, it was suggested that a novel ESCRT-III-like

complex could be involved in the surveillance of nuclear pore complex (NPC) assembly at the nuclear membrane in yeast (Webster *et al.* 2014), but it is not clear whether this complex contains a CHMP7 ortholog.

In several publications, it has been claimed that there is no yeast ortholog of CHMP7 (Row *et al.* 2007; Kieffer *et al.* 2008; Hurley and Hanson 2010). This notion is based on a misquotation of the paper by Horii *et al.* (2006) because these authors clearly show that there is a yeast homolog of CHMP7. We name this protein, encoded by yeast ORF YJL049w, Chm7. CHMP7 is found in the genomes of most eukaryotic taxa (Leung *et al.* 2008). This suggests that CHMP7 is also a very ancient component of the ESCRT machinery, which was possibly already present in the "last common eukaryotic ancestor." Our data point to a role of Chm7 at the endoplasmic reticulum (ER), possibly as part of an alternative ESCRT-III-like complex.

## Materials and Methods

### Strains and plasmids

Yeast cells were either grown in YPD medium (1% yeast extract, 2% Bacto Peptone, and 2% glucose) or in SD/CAS medium (0.67% yeast nitrogen base, 1% casamino acids, and 2% glucose) to select for the presence of plasmids (with a *URA3* or *TRP1* marker). The yeast strains used are listed in Table 1. The strains are derived from the wild-type strain JD52 (J. Dohmen, Köln, Germany). The coding sequences for epitope tags and gene deletions were introduced into the yeast genome by homologous recombination with PCR-generated cassettes (Longtine *et al.* 1998). The correct integration of the cassettes was verified by PCR. The genotypes of the plasmids used are listed in Table 2. The cloned genes were amplified with Phusion DNA Polymerase (Thermo Scientific, Schwerte, Germany) from chromosomal DNA of JD52. The amplified genes were verified by sequencing (GATC Biotech, Konstanz, Germany) to exclude PCR errors. The MIM1 sequence in *CHM7* was deleted by QuikChange PCR mutagenesis (Agilent, Waldbronn, Germany).

### Gal depletion

For gal-depletion experiments, yeast strains transformed with pRK505, coding for a myc-tagged version of *STE6* under the control of the *GAL1* promoter, were grown overnight to exponential phase ($OD_{600} < 1.0$ or $<5 \times 10^7$/ml) in SD/CAS medium with 2% galactose. At time $t_0$, cells were spun down and resuspended in SD/CAS medium with 2% glucose, and aliquots were taken at time intervals and analyzed by Western blotting with anti-myc antibodies.

### Differential centrifugation

Yeast cells were grown overnight in YPD or SD/CAS medium to exponential phase ($OD_{600} < 1.0$ or $<5 \times 10^7$/ml). All further steps were performed with ice-cold solutions. Then 10 $OD_{600}$ cells were harvested, washed with 10 mM $NaN_3$, resuspended in 200 μl of lysis buffer (LB; 50 mM HEPES, pH 7.5, 300 mM sorbitol, and 10 mM $NaN_3$) + protease inhibitors, and broken by glass-bead lysis for 5 min at 4°. After addition of 600 μl LB, the liquid was taken off and spun at 500 × *g* for 5 min to remove cell debris. A 50-μl aliquot of the cleared lysate was retained as a control (total fraction). Then 500 μl of the cleared lysate was centrifuged at 13,000 × *g* for 10 min in a tabletop centrifuge at 4°. The pellets from the 13,000 × *g* spin were carefully resuspended in 500 μl LB (P13 fraction), and the supernatants were centrifuged again at 100,000 × *g* for 1 hr at 4° in a Sorvall Discovery M120SE ultracentrifuge with an S45-A rotor. The supernatants from the 100,000 × *g* spin were removed (S100 fraction), and the pellets were again resuspended in 500 μl LB (P100 fraction). One set of experiments was performed with cleared lysates that were incubated on ice for 30 min with 1% Triton X-100 before centrifugation to solubilize the membranes. The fractions were analyzed by Western blotting with specific antibodies.

**Table 2 Plasmids**

| Plasmid | Genotype |
|---|---|
| pACT2[a] | *2μ GAL-AD LEU2* |
| pRK329 | *2μ GAL-BD TRP1* |
| pRK505 | *CEN/ARS GAL1p-STE6myc TRP1* |
| pRK581 | *2μ GAL-BD-MOS10/VPS60 TRP1* |
| pRK642 | *2μ GAL-BD-VPS4 TRP1* |
| pRK770 | *2μ SNF7-GFP URA3* |
| pRK842 | *2μ GAL-BD-VPS20 TRP1* |
| pRK942 | *2μ GAL-BD-SNF7 TRP1* |
| pRK1157 | *2μ CHM7-GFP URA3* |
| pRK1216 | *2μ GAL-AD-CHM7 LEU2* |
| pRK1263 | *2μ HXT7p-mCherry-CHM7 TRP1* |
| pRK1266 | *2μ CHM7-mCherry URA3* |
| pRK1332 | *2μ HXT7p-yEGFP-CHM7 TRP1* |
| pRK1405 | *CEN/ARS HXT7p-yEGFP-CPS1 TRP1* |
| pRK1436 | *2μ CHM7ΔMIM1-mCherry (aa 414–421 deleted) URA3* |
| pRK1464 | *CEN/ARS CHM7-3HA URA3* |
| pRK1511 | *CEN/ARS CHM7ΔMIM1 (aa 414–421 deleted) ADH1$_t$ TRP1* |
| pRK1514 | *2μ HMG1 URA3* |
| pRK1516 | *CEN/ARS CHM7 ADH1$_t$ TRP1* |
| pRK1531 | *2μ GAL-BD-IST1 TRP1* |
| pRK1532 | *2μ GAL-BD-DID2 TRP1* |
| pRK1533 | *2μ GAL-BD-DID4/VPS2 TRP1* |
| pRK1534 | *2μ GAL-BD-VPS24 TRP1* |
| pRK1536 | *2μ GAL-BD-VTA1 TRP1* |
| pRK1651 | *2μ-DID2-mCherry URA3* |
| pRK1652 | *2μ-IST1-mCherry URA3* |
| pRK1653 | *2μ-MOS10-mCherry URA3* |
| pRK1654 | *2μ-SNF7-mCherry URA3* |
| pRK1655 | *2μ-VPS2-mCherry URA3* |
| pRK1656 | *2μ-VPS20-mCherry URA3* |
| pRK1657 | *2μ-VPS24-mCherry URA3* |
| pRK1659 | *2μ-HMG1 TRP1* |

[a] Clontech, Palo Alto, CA.

### Sucrose density gradient fractionation

Yeast cells were grown overnight in YPD medium to exponential phase ($OD_{600} < 1.0$ or $<5 \times 10^7$/ml). All further steps were performed with ice-cold solutions. About 50 $OD_{600}$ cells were harvested, washed with 10 mM $NaN_3$, resuspended in 100 μl STE10 buffer (10% by mass sucrose, 10 mM Tris-Cl, pH 7.6, and 1 mM EDTA) + protease inhibitors, and broken by glass-bead lysis for 5 min at 4°. After addition of 500 μl STE10, the liquid was taken off and spun at

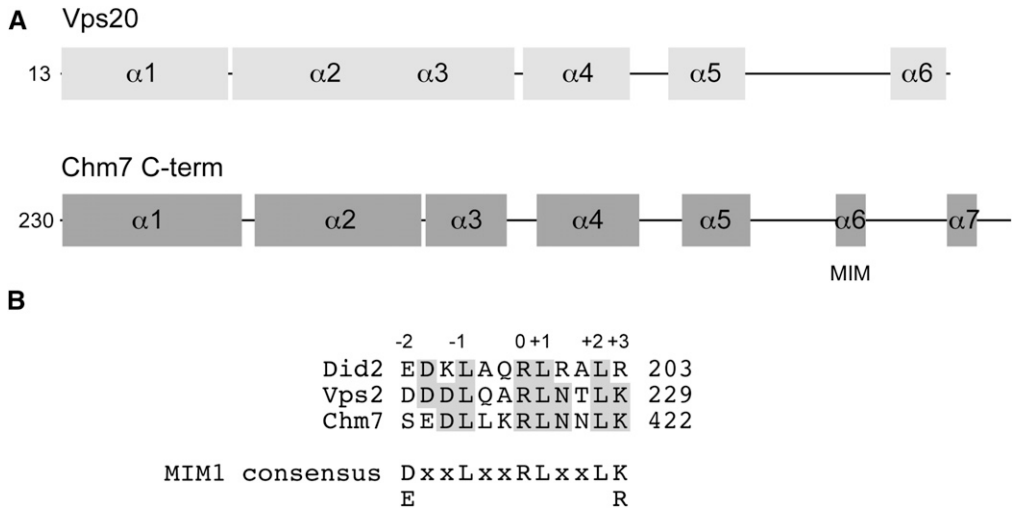


**Figure 1** Chm7 contains an ESCRT-III domain. (A) Secondary-structure analysis with Jpred (http://www.compbio.dundee.ac.uk/www-jpred/) of Vps20 (top) and of the C-terminal half of Chm7 (bottom). The numbers on the left indicate the sequence position. (B) Chm7 contains a MIM1 motif in helix α6. Alignment of Chm7 with the MIM1 motifs of Did2 and Vps2; MIM1 consensus sequence as defined in Obita *et al.* (2007) and Stuchell-Brereton *et al.* (2007).

500 × *g* for 5 min to remove cell debris. About 400 μl of the cleared lysate was loaded onto the sucrose gradient, which was prepared in the following way: 1.7 ml each of STE53 (53% by mass sucrose), STE35 (35% by mass sucrose), and STE20 (20% by mass sucrose) in 10 mM Tris-Cl (pH 7.6) and 1 mM EDTA was overlayed in a 5-ml ultracentrifuge tube. The sealed tube was placed in a horizontal position for 3 hr at 4° and then was returned to the vertical position. Then 400 μl was removed from the top, and the cell extract was applied to the gradient. The tubes were centrifuged for 14 hr at 100,000 × *g* at 4° in a Sorvall Discovery M120SE ultracentrifuge with an S52-ST rotor. After centrifugation, eighteen 280-μl fractions were carefully removed from the top with a Gilson pipette. The fractions were analyzed by Western blotting with specific antibodies against marker proteins.

### *Fluorescence microscopy*

Yeast cells were grown overnight in SD/CAS medium to exponential phase ($OD_{600} < 1.0$ or $< 5 \times 10^7$/ml). Then 1 ml of the culture was mixed with DAPI (1 mg/ml in water) and incubated 10 min further at 30° with shaking. Then 50 μl of the cell suspension was mixed with 50 μl of 2% low-melt agarose held at 50°. The mixture was put on a glass slide and examined with a Zeiss Axio-Imager M1 fluorescence microscope equipped with an AxioCam MRm camera (Zeiss, Göttingen, Germany). Images were acquired with AxioVision software and processed with Photoshop Elements.

### *Data availability*

Strains are available upon request.

## Results

### *Saccharomyces cerevisiae contains a CHMP7 ortholog*

It has been claimed in several publications that the yeast *S. cerevisiae* does not contain an ortholog of the human ESCRT-III-related protein CHMP7 (Row *et al.* 2007; Kieffer *et al.* 2008; Hurley and Hanson 2010). Curiously, these publications refer to the original paper on human CHMP7, in which just the opposite was stated (Horii *et al.* 2006). The yeast counterpart of CHMP7, which we name Chm7 in analogy to the human protein, consists of 450 amino acids (CHMP7: 453 amino acids). The secondary structure of the C-terminal half of Chm7, as predicted by JPred (Cole *et al.* 2008), is highly similar to the secondary structure of canonical ESCRT-III proteins (Figure 1A), and the Pfam database (Finn *et al.* 2014) predicts that Chm7 belongs to the Snf7 protein family.

To further corroborate these findings, we looked for homologous domains in Chm7 with the HHPred algorithm (Remmert *et al.* 2012). HHPred is a highly sensitive tool for the identification of related proteins or protein families. HHPred identified the ESCRT-III protein Vps20 as the best match to the Chm7 C-terminus. The program calculates the probability for a true match, which in this case was 99.95, *i.e.*, close to certainty (Prob = 100). A startling result was obtained for the N-terminal half of Chm7. HHPred predicted that the N-terminal half of Chm7 is related to the ESCRT-II protein Vps25 (Prob = 96.84). This finding is intriguing because Vps25 is the ESCRT-II component that recruits ESCRT-III via interaction with Vps20 (Saksena *et al.* 2009). ESCRT-II contains two subunits of Vps25 that nucleate the formation of two Snf7 filaments (via Vps20 binding). Thus, our findings suggest that Chm7 is an in-frame fusion of two proteins, similar to the ones that mediate the ESCRT-II–ESCRT-III interaction.

On closer inspection of the Chm7 sequence, we noticed the presence of an MIM1 consensus motif close to the C-terminus (Figure 1B). MIM1 motifs are present in some of the ESCRT-III proteins (*e.g.*, Did2 and Vps2) and bind to MIT domains (Obita *et al.* 2007; Stuchell-Brereton *et al.* 2007). The presence of such a motif in Chm7 further highlights the ESCRT-III-like character of the C-terminal half of Chm7.

### *Chm7 is not involved in the degradation of endocytic cargo proteins*

Horii *et al.* (2006) concluded that human CHMP7, like the canonical ESCRT-III complex, functions in the endosomal sorting pathway. To test whether this is true for the yeast counterpart, we examined the turnover of a cargo protein

for the endosomal sorting pathway in a *CHM7* deletion mutant. This cargo protein, the a-factor transporter Ste6, travels to the cell surface and is internalized rapidly by endocytosis and then is directed to the multivesicular body (MVB) pathway in a ubiquitination-dependent manner for its final degradation in the yeast vacuole (Kölling and Hollenberg 1994). The Ste6 half-life was determined by a gal-depletion experiment, where *STE6* expression from the *GAL1* promoter was shut off at $t_0$ by a shift in carbon source from galactose to glucose.

Ste6 turnover was examined in deletion mutants of all ESCRT-III family members and in a *VTA1* deletion mutant. Vta1 was included in the analysis because it displays a two-hybrid interaction with Chm7 (see later). In the wild-type strain, Ste6 had a short half-life of 16 min (Figure 2), as reported previously (Kölling and Hollenberg 1994), while it was strongly stabilized in all classical ESCRT-III family member mutants (*Δdid2*, *Δmos10*/*Δvps60*, *Δsnf7*, *Δvps2*, *Δvps20*, and *Δvps24*) and in the *VTA1* mutant. Despite the strong stabilization, Ste6 was not completely stable in any of the mutants. This could mean that either ESCRT-III is not absolutely essential for Ste6 degradation or that individual ESCRT-III proteins perform partially redundant functions. Interestingly, deletion of *VPS24* seemed to have a stronger impact on Ste6 turnover than deletion of the other ESCRT-III family members. This may indicate that Vps24 plays a more prominent role in the ESCRT-III system, *e.g.*, by acting as a component in different redundant ESCRT-III complexes. The Ste6 half-lives in some of the mutants showed a high degree of variability. We think that this is not due to technical problems because the quality of the data generally was high (correlation coefficients close to 1). Also, the wild-type strain did not show this variability.

In contrast to the classical ESCRT-III deletions, no stabilization of Ste6 was observed in mutants lacking the noncanonical ESCRT-III members Chm7 and Ist1. Also, Ste6 was not stabilized in a *Δchm7 Δist1* double mutant. The turnover seemed to be even higher in the double mutant compared to single mutants.

To substantiate our findings, the intracellular distribution of another cargo protein of the vacuolar protein sorting pathway, GFP-CPS, was examined by fluorescence microscopy. GFP-CPS is sorted to the vacuolar lumen in the wild-type strain, while in ESCRT mutants it accumulates in the vacuolar membrane and in patchlike structures close to the vacuole (class E compartment) (Raymond *et al.* 1992), presumably consisting of dilated late endosomes (Rieder *et al.* 1996).

The observed staining patterns are perfectly in line with our gal-depletion experiments (Figure 3). In the classical ESCRT-III mutants (*Δdid2*, *Δmos10*, *Δsnf7*, *Δvps2*, *Δvps20*, and *Δvps24*), a class E staining pattern was observed, while in wild-type and *Δchm7* strains and in the *Δchm7 Δist1* double mutant, GFP-CPS luminal staining was obtained. The *Δist1* mutant showed an intermediate phenotype. We saw mostly luminal staining with some occasional dotlike structures. With this information taken together, we conclude that Chm7 does not appear to play an essential role in the degradation of proteins via the MVB pathway.

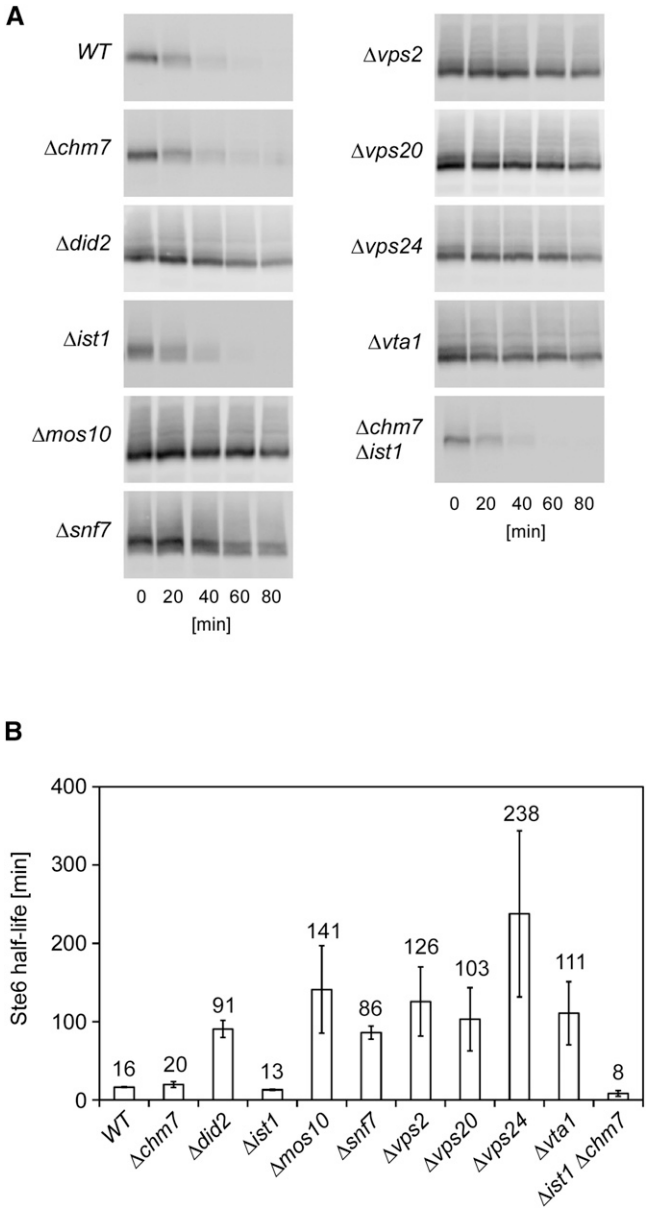


**Figure 2** Ste6 half-life in ESCRT-III mutants. Different ESCRT-III mutants were transformed with plasmid pRK505 expressing Ste6-myc from the *GAL1* promoter, and the Ste6 half-life was determined by a gal-depletion experiment. (A) Aliquots of the cultures were taken at the times indicated and analyzed by Western blotting with anti-myc antibodies. The ESCRT-III mutants were (top left to bottom right) JD52 (wild type), RKY2468 (*Δchm7*), RKY1728 (*Δdid2*), RKY2681 (*Δist1*), RKY1509 (*Δmos10*), RKY1510 (*Δsnf7*), RKY1732 (*Δvps2*), RKY1590 (*Δvps20*), RKY1730 (*Δvps24*), RKY2755 (*Δvta1*), and RKY2757 (*Δchm7 Δist1*). (B) The Ste6 Western blot signals were quantified with the program GelAnalyzer 2010a, and the Ste6 half-lives in the different mutants were calculated as indicated (average of three independent experiments with SDs).

### *Chm7 does not behave like a typical ESCRT-III protein*

To further prove or disprove a role of Chm7 in endosomal sorting, we compared the behavior of Chm7 and Snf7 in

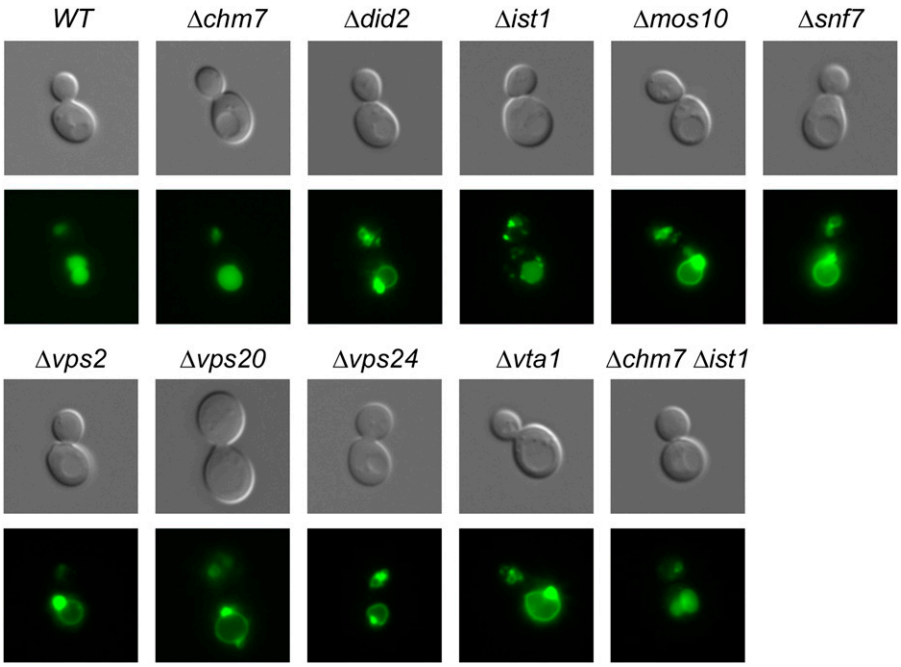


**Figure 3** Localization of GFP-CPS in ESCRT-III mutants. Different ESCRT-III mutants were transformed with plasmid pRK1405 expressing yEGFP-Cps1 from the *HXT7* promoter. yEGFP staining was observed with the fluorescence microscope. The same strains as in Figure 2 were used (from left to right). (Top panels) DIC image. (Bottom panels) yEGFP fluorescence.

biochemical fractionation experiments. ESCRT-III is assembled at the endosomal membrane. Under steady-state conditions, Snf7 is mostly soluble, and only a smaller fraction of the protein is membrane associated (Babst *et al.* 2002a). It is thought that ESCRT complexes are disassembled and released from the endosomal membrane through the action of the AAA-ATPase Vps4 (Babst *et al.* 1998). In a *Δvps4* mutant, ESCRT complexes, as well as cargo proteins, accumulate in the class E compartment. To test whether Chm7 behaves similarly to the central ESCRT-III component Snf7 with respect to membrane association and class E compartment accumulation, a differential centrifugation experiment was performed. Cell extracts of a yeast strain expressing a C-terminal 3HA-tagged Chm7 variant from the chromosomal copy of the gene were fractionated by sequential centrifugation at 13,000 and 100,000 × *g* (Figure 4A). The tagged protein was functional (see later for the assay). Larger organelles or membrane structures (*e.g.*, plasma membrane fragments, ER, mitochondria, and vacuolar membranes) sediment into the P13 pellet, while smaller structures (*e.g.*, Golgi apparatus, vesicles, and part of the endosomal fraction) are found in the P100 pellet. Soluble proteins remain in the S100 supernatant. In a parallel experiment, cell extracts were treated with the detergent Triton X-100 prior to centrifugation to solubilize the membranes.

With extracts from a wild-type strain, 40% of Snf7 was recovered in the pellet fractions, about equally distributed between the P13 and P100 pellets. About half the P13 fraction (10% of total Snf7) could be solubilized by detergent treatment. The P100 pool proved to be fairly Triton resistant (Figure 4B). From this we conclude that at least 10% of Snf7 is membrane associated under these conditions. The remaining protein in the P13 and P100 fractions could be associated with detergent-resistant membranes (DRMs, or rafts) or could be part of a larger protein particle (ESCRT-III filaments?) or part of protein aggregates. It has been observed previously that ESCRT-III complexes are largely resistant to nonionic detergents (Bodon *et al.* 2011).

*VPS4* deletion had a strong impact on the Snf7 fractionation pattern (Figure 4B). In line with previous work (Babst *et al.* 2002a), Snf7 was now almost completely localized to the pellet fractions. Detergent treatment strongly reduced the amount of Snf7 in the P13 fraction. The protein extracted from P13 did not show up in the soluble fraction but was instead recovered in the P100 fraction. A possible explanation for this fractionation behavior could be that the detergent-extracted endosomal ESCRT complexes in *Δvps4* are too large to be soluble.

The fractionation pattern of Chm7 with wild-type extracts resembled the Snf7 pattern (Figure 4C). About half the protein was found in P13 and P100, again distributed about equally between the two fractions. About half the P13 and P100 pools could be extracted by Triton X-100 (28% of total Chm7). This indicates that at least 28% of Chm7 is membrane associated under normal conditions. The main difference between Chm7 and Snf7, though, was their Vps4 dependence. In contrast to Snf7, Chm7 membrane association was not significantly affected by loss of *VPS4*. Likewise, deletion of the MIM1 sequence in Chm7 had no effect on its membrane association (not shown).

To take a closer look at the Chm7 distribution in wild-type and *Δvps4* strains, cell extracts were fractionated on sucrose gradients. The Chm7 distribution was compared with the distribution of endosomal marker proteins (Pep12 and Snf7) and the distribution of ER/*cis*-Golgi markers (Dpm1 and Emp47). The proteins were detected by Western blotting with specific antibodies. Quantification of the Western blot signals is presented in Figure 5.

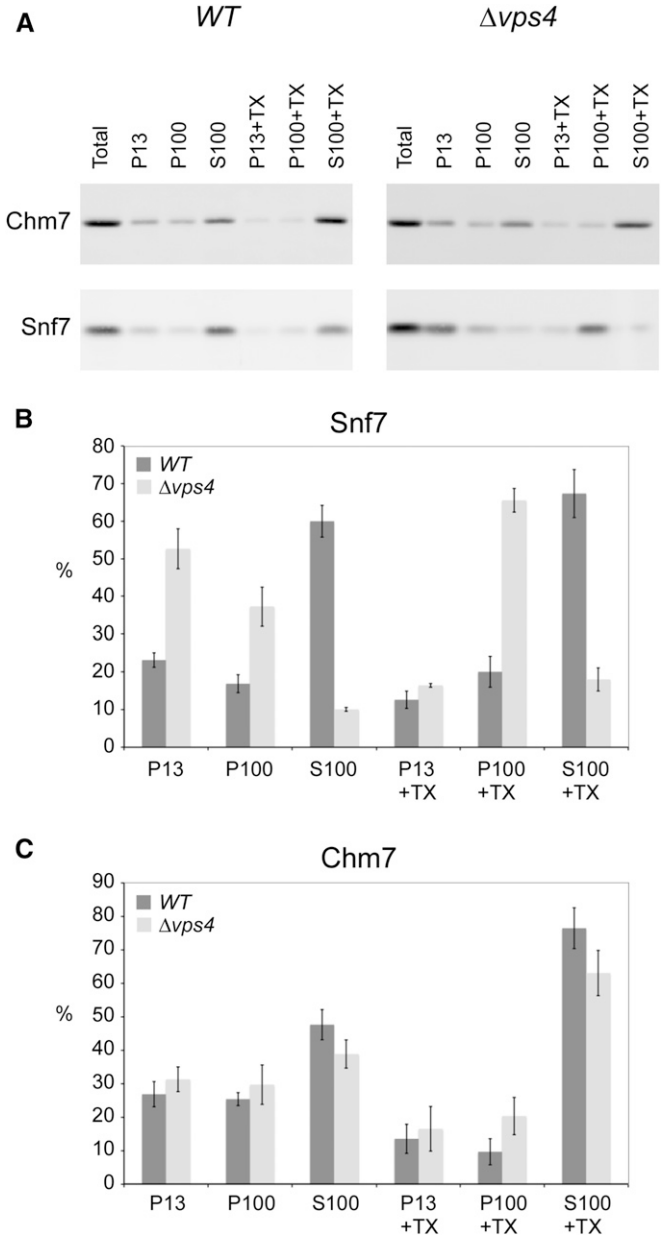


**Figure 4** Chm7 membrane association does not depend on Vps4. The membrane association of Chm7-3HA and Snf7 was examined by differential centrifugation. (A) Cell extracts of RKY2302 (wild type) (left panels) and RKY2495 (*Δvps4l*) (right panels) were separated into P13 and P100 pellet fractions and into the S100 supernatant fraction. As a control, the corresponding amount of the total fraction was loaded ("Total"). Cell extracts were either treated with Triton X-100 (+TX) or left untreated. The fractions were analyzed by Western blotting with either anti-HA antibodies (Chm7-3HA) (top panels) or anti-Snf7 antibodies (bottom panels). The Western blot signals were quantified with ImageJ. (B) Snf7. (C) Chm7-3HA. The sum of P13 + P100 + S100 was set to 100%. Dark-gray bars, wild type; light-gray bars, *Δvps4*. (Right) Triton X-100 treatment (+TX). (Left) Untreated. Number of experiments: wild type ($n$ = 4), *Δvps4* ($n$ = 3).

With wild-type extracts, the late endosome marker Pep12 formed a peak in fractions 6–8, which probably represents an overlap of two fractions with slightly different densities (Figure 5A). In line with the differential centrifugation experiment, most of the Snf7 was found in the soluble protein fraction (fraction 2). The rest of the Snf7 was broadly distributed along the gradient, partially overlapping with the Pep12 peak. The Chm7 distribution resembled neither the Pep12 nor the Snf7 distribution. It was detected in a broad peak at the top of the gradient between fractions 2 and 6. This peak represents an overlap between the soluble Chm7 protein around fraction 2 (about 50% of the total protein, according to the differential centrifugation experiment) and another low-density compartment (peak in fraction 6).

The fractionation pattern changed dramatically with cell extracts from the *Δvps4* mutant (Figure 5B). Now both endosomal markers, Pep12 and Snf7, were detected in a single peak (fraction 9), the class E peak. The Chm7 distribution, however, barely changed. Most notably, Chm7 did not accumulate in the class E peak, which would have been expected for a canonical ESCRT-III protein. Thus, Chm7 behaves very differently from the ESCRT-III component Snf7.

Instead, the Chm7 distribution closely resembled the distribution of the ER/*cis*-Golgi markers Dpm1 and Emp47 (Figure 5C). These markers showed a complex fractionation pattern with peaks in fractions 5–6, 9, and 13, with the main peak in fraction 5–6. These peaks could correspond to different subcompartments of the ER/Golgi system. With cell extracts from the *Δvps4* strain, the fractionation pattern of the three proteins did not change much (Figure 5D). The only difference that could be observed was a loss of the minor peak in fraction 9 for Dpm1 and Emp47. In effect, the Chm7 distribution now resembled the distribution of Dpm1 and Emp47 even more closely (except for the shoulder of soluble protein around fraction 2).

### *Chm7 localization*

Our sucrose gradient fractionation is compatible with an ER localization of Chm7. To further substantiate this notion, we looked at the intracellular distribution of Chm7 fusions N- or C-terminally tagged with the fluorescent protein mCherry. The mCherry fusions were functional (see later for the assay). The fluorescence was more or less evenly distributed in the cytoplasm and was excluded from the vacuole and the nucleus (Figure 6A). In some cells, the mCherry staining appeared to be somewhat brighter around the nucleus (see upper row in Figure 6A). Next, we were interested to see how deletion of the MIM1 motif affects Chm7 localization. With the Chm7ΔMIM-mCherry variant, the staining was no longer evenly distributed in the cytoplasm but was instead concentrated in about half a dozen dots or patches per cell. In addition, staining around the vacuole was discernible in about half the cells (Figure 6B). A similar staining pattern was obtained with wild-type Chm7-mCherry in a *Δvps4* mutant (Figure 6C). The only difference was that the ringlike vacuolar staining was observed only rarely (<10% of cells) and that the dots appeared to be somewhat brighter.

We wondered whether the observed Chm7ΔMIM-mCherry dots are derived from the ER. To test this, we coexpressed Chm7-mCherry and Chm7ΔMIM-mCherry with the ER marker Sec63-GFP expressed from the chromosomal copy

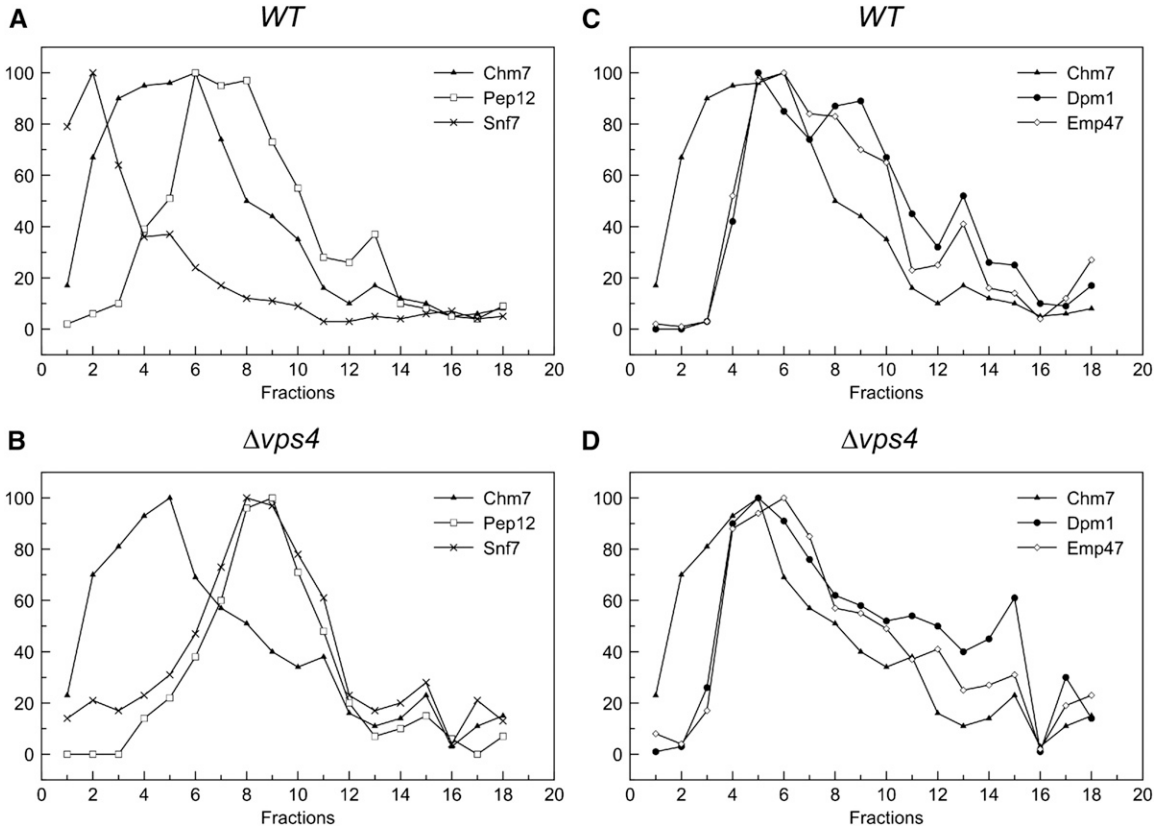


**Figure 5** Fractionation of Chm7-3HA on sucrose gradients. Cell extracts of the strains RKY2302 (*CHM7-3HA*) (A and C) and RKY2495 (*CHM7-3HA Δvps4*) (B and D) were fractionated on sucrose gradients. Fraction 1 = low density; fraction 18 = high density. The fractions were analyzed by Western blotting with specific antibodies against Chm7-3HA, Dpm1, Emp47, Pep12, and Snf7. The Western blot signals were quantified with the program ImageJ. The strongest signal for each protein was set to 100. (A and B) Chm7-3HA (closed triangles), Pep12 (open squares), and Snf7 (crosses). (C and D) Chm7-3HA (closed triangles), Dpm1 (closed circles), and Emp47 (open diamonds).

of the gene (Figure 6D). For Sec63-GFP, a typical ER pattern was observed, with perinuclear rings and cortical staining. In some Chm7-mCherry-expressing cells, again the mCherry staining appeared to be somewhat brighter in the area of perinuclear Sec63-GFP staining, in line with the supposed ER localization of Chm7. The Chm7ΔMIM-mCherry dots, however, did not colocalize with Sec63-GFP. Thus, they are probably not derived from the ER, or the ER-derived structures are devoid of Sec63-GFP.

The large soluble pool of Chm7 could obscure the ER staining. We figured that disturbing the ER membrane structure might lead to a clearly discernible change in the Chm7 staining pattern. To this end, we overexpressed the gene for HMG-CoA reductase, which leads to the formation of spectacular ER-derived membrane structures called *karmellae* (Wright *et al.* 1988). Karmellae are onionlike ER membrane stacks wrapped around the nucleus. On coexpression of our *mCherry-CHM7* construct, we could indeed observe brightly staining mCherry-Chm7 rings around the nucleus (Figure 7), supporting an ER localization of Chm7-mCherry.

To test whether karmellae localization is specific for Chm7, *HMG1* was overexpressed in strains expressing C-terminal mCherry-tagged versions of all ESCRT-III proteins (Figure 7). Because karmellae are induced only in some cells expressing Hmg1 to very high levels, most cells display the normal localization of the ESCRT-III mCherry fusions. Perinuclear rings could be identified only in cells expressing Vps2 and Vps20. Thus, perinuclear localization is not a general feature of ESCRT-III proteins. The Vps2-mCherry staining was generally very faint and resembled the Chm7-mCherry staining. The Vps20-mCherry staining in normal cells (without karmellae) consisted of a faint class E staining. A similar, more intensive class E staining was observed with Mos10- and Snf7-mCherry. Did2- and Vps24-mCherry showed a number of dots close to the vacuole, presumably corresponding to endosomes. An unexpected staining pattern was observed for Ist1-mCherry. The protein was exclusively localized inside the nucleus. This result was obtained with several independent transformants.

In summary, our data are consistent with the notion that at least a fraction of Chm7 is associated with the ER under normal conditions.

### *Chm7 interacts with other ESCRT-III proteins*

To investigate whether Chm7 functions as part of an ESCRT-III-like complex, the other yeast ESCRT-III or ESCRT-III-like proteins were examined for protein-protein interactions with Chm7 by two-hybrid analysis (Figure 8). The MIT-domain

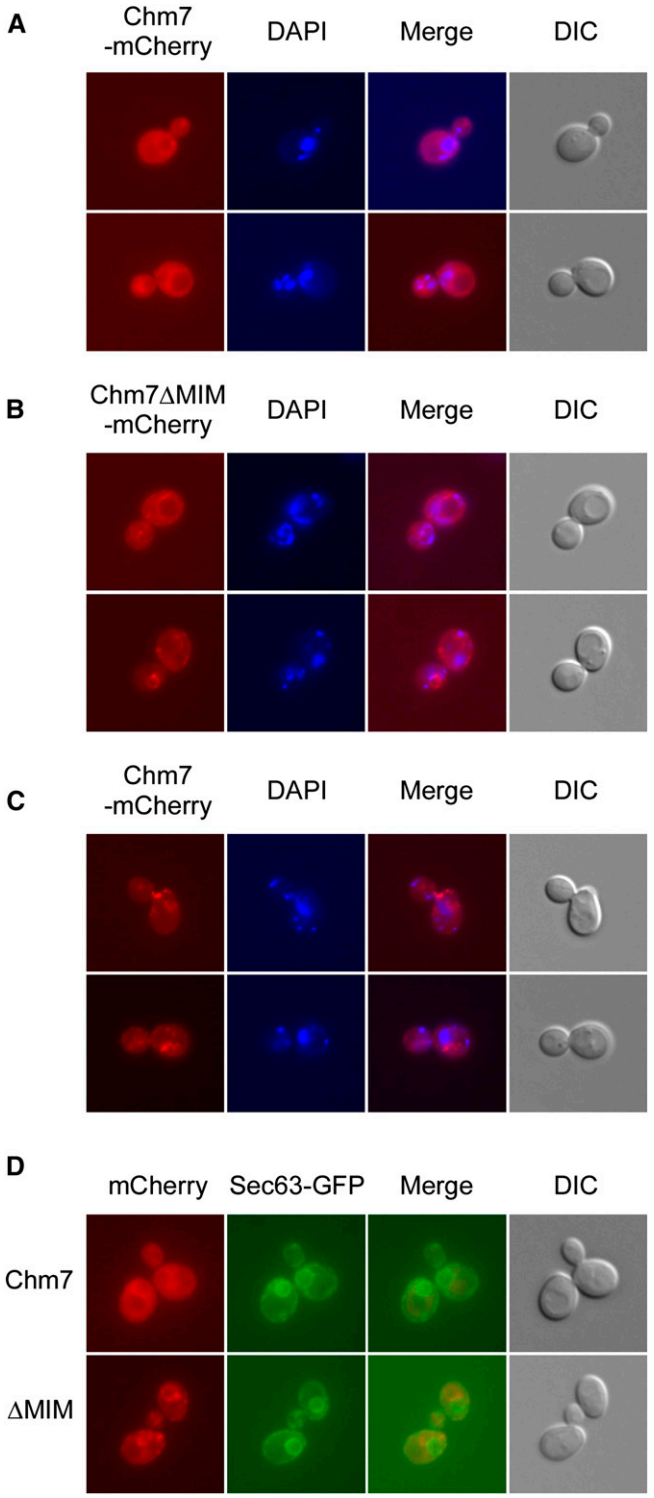


**Figure 6** Intracellular localization of Chm7-mCherry fusions. (A) JD52/pRK1266 (*CHM7-mCherry*). (B) JD52/pRK1436 (*CHM7ΔMIM1-mCherry*). (C) RKY1511 (*Δvps4*)/pRK1266 (*CHM7-mCherry*). Columns (from left to right): mCherry staining, DAPI staining (nuclei and mitochondria), merged image, and DIC image. (D) RKY2725 (*SEC63-GFP*)/pRK1266 (*CHM7-mCherry*) (top panels) and RKY2725 (*SEC63-GFP*)/pRK1436 (*CHM7ΔMIM1-mCherry*) (bottom panels). Columns (from left to right): mCherry staining, GFP staining, merged image, and DIC image.

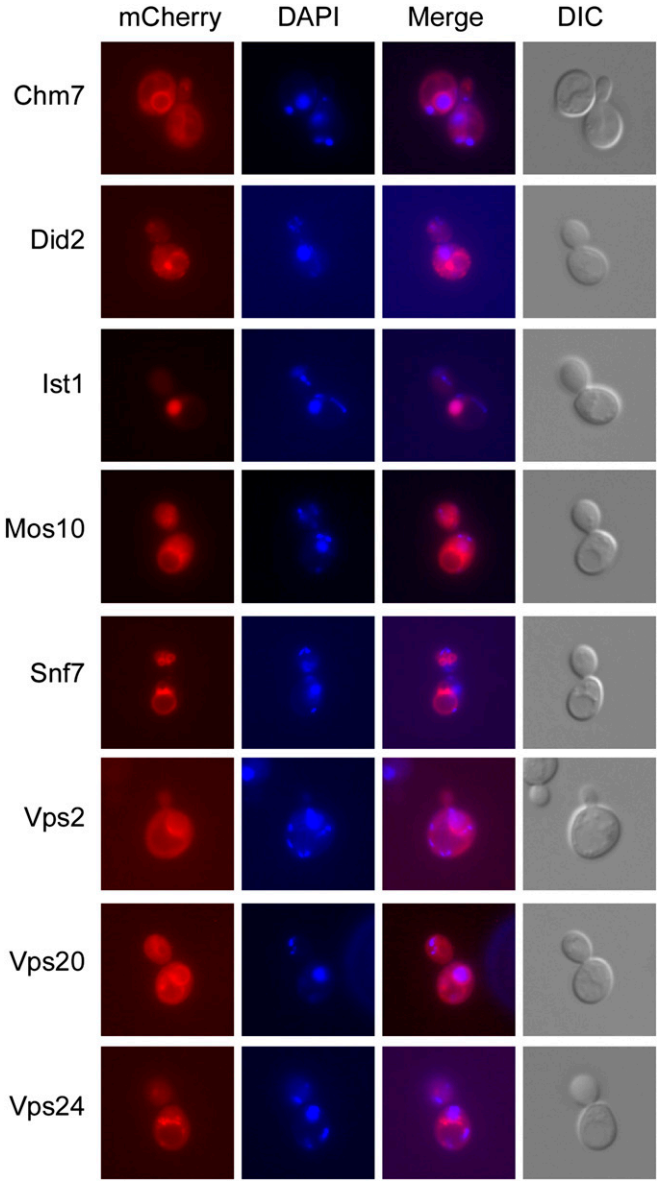


**Figure 7** Effect of HMG-CoA reductase overexpression on the localization of ESCRT-III proteins. The wild-type strain JD52 was transformed with the *HMG1*-overexpressing plasmid pRK1659 and with 2μ-plasmids expressing ESCRT-III–mCherry fusions. The ESCRT-III proteins are (from top to bottom) Chm7 (pRK1266), Did2 (pRK1651), Ist1 (pRK1652), Mos10 (pRK1653), Snf7 (pRK1654), Vps2 (pRK1655), Vps20 (pRK1656), and Vps24 (pRK1657). Columns (from left to right): mCherry staining, DAPI staining (nuclei and mitochondria), merged image, and DIC image.

proteins Vps4 and Vta1 were included in the analysis. Chm7 was fused to the Gal4 activation domain (Gal-AD), and the putative binding partners were fused to the Gal4 DNA binding domain (Gal-BD). Interaction between two fusions leads to an activation of the *HIS3* reporter gene and thus to growth on −his plates. Activation was observed with Gal-BD-Snf7, -Vps2, -Ist1, and -Vta1 in combination with Gal-AD-Chm7. The Gal-BD fusions with Did2, Mos10/Vps60, Vps20, Vps24, and Vps4 did not interact. This suggests that Chm7

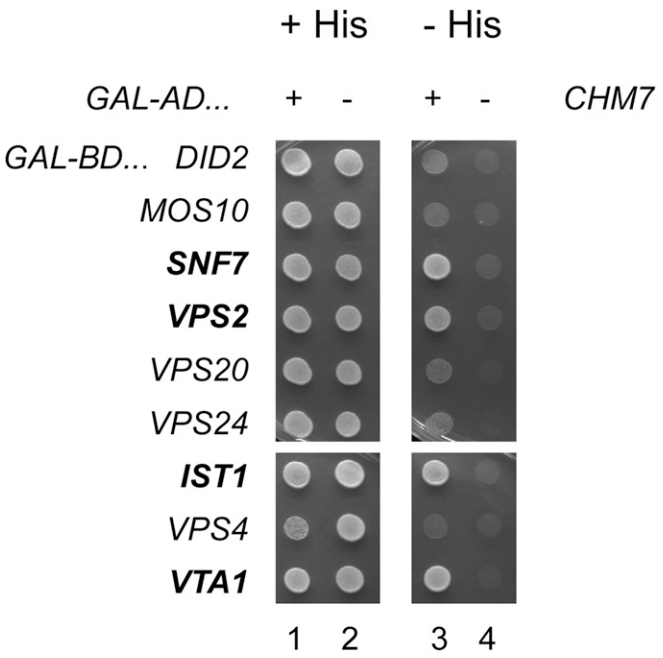


**Figure 8** Two-hybrid analysis of Chm7–ESCRT-III interactions. The two-hybrid tester strain PJ69-4A was transformed with the *GAL-AD-CHM7* plasmid pRK1216 (1 and 3) or the pACT2 vector control (2 and 4) and with different *GAL-BD* fusions. (From top to bottom) pRK1532 (*DID2*), pRK581 (*MOS10/VPS60*), pRK942 (*SNF7*), pRK1533 (*DID4/VPS2*), pRK842 (*VPS20*), pRK1534 (*VPS24*), pRK1531 (*IST1*), pRK642 (*VPS4*), and pRK1536 (*VTA1*). Cell suspensions were spotted onto SD plates containing histidine (+His) (1 and 2) and onto plates without histidine (−His) (3 and 4) and incubated for 3 days at 30°C.

could be part of an alternative ESCRT-III-like complex containing Snf7, Vps2, and Ist1.

We also tried to detect the Chm7 interactions by coimmunoprecipitation, but these attempts were not successful (not shown). As an alternative way to test for an *in vivo* interaction, mCherry-Chm7 and Snf7-GFP were coexpressed in a wild-type yeast strain. Fusion of GFP to the C-terminus of Snf7 blocks autoinhibition and disassembly of the ESCRT-III complex at the endosomal membrane (Teis *et al.* 2008), leading to a class E phenotype, *i.e.*, accumulation of cargo proteins and Snf7-GFP in a brightly staining dotlike structure at the vacuolar membrane together with some staining of the vacuolar membrane. Both fusions were expressed from multicopy plasmids. In cells with a lower Snf7-GFP expression level, a typical class E staining was observed for Snf7 (Figure 9, bottom row). The mCherry-Chm7 staining seemed to be unaffected by Snf7-GFP expression, and no colocalization between the two proteins was detected. However, in cells with high Snf7-GFP expression levels, brightly stained filamentous structures were observed between the nucleus and the vacuole (Figure 9, top two rows). These structures were also stained for mCherry-Chm7. Thus, it appears that Snf7 is able to sequester Chm7 when present in large excess. This shows that, in principle, Snf7 is able to bind to Chm7 *in vivo*. These findings point to the existence of an alternative ER-localized ESCRT-III complex that contains Chm7 as a subunit.

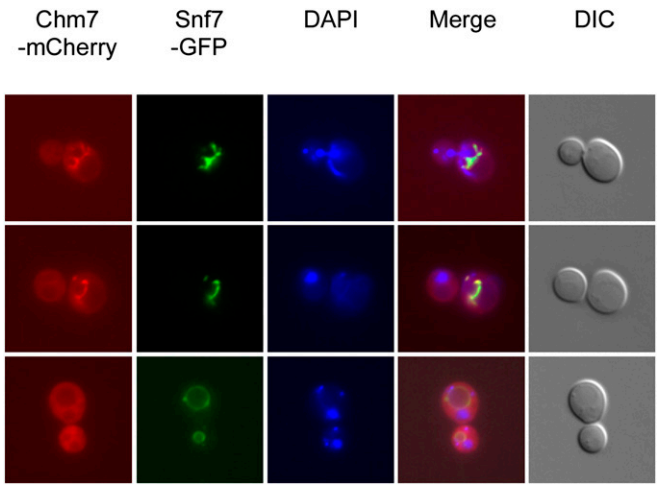


**Figure 9** Colocalization between Chm7 and Snf7. JD52 was transformed with pRK1263 (*mCherry-Chm7*) and pRK770 (*SNF7-GFP*). Columns (from left to right): mCherry staining (Chm7), GFP staining (Snf7), DAPI staining (nuclei and mitochondria), merged image, and DIC image.

### *Synthetic lethal interaction between Δchm7 and Δapq12*

BIOGRID (http://thebiogrid.org/) lists 30 genetic interactions with the *CHM7* deletion. At least nine of them can be linked to ER function (*APQ12*, *CPR8*, *EUG1*, *ICE2*, *SEC61*, *SEC63*, *SEC66*, *SPF1*, and *THP2*). We decided to take a closer look at the *Δchm7-Δapq12* interaction (Figure 10A). Apq12 has been linked to NPC assembly and to messenger RNA (mRNA) export from the nucleus (Baker *et al.* 2004; Scarcelli *et al.* 2007). As noted previously (Scarcelli *et al.* 2007), the strains containing the *Δapq12* deletion had a growth defect at low temperature (20°). The *CHM7* deletion strain grew like the wild-type strain at this temperature. At 30°, all mutants exhibited wild-type growth. At 37°, however, the *Δchm7 Δapq12* double mutant showed a growth defect, while the single mutants grew like the wild-type strain. This demonstrates that *CHM7* is required for optimal growth at 37° in a *Δapq12* background. This is the first phenotype that we could detect for the *CHM7* deletion in yeast. The temperature-sensitive phenotype of the double mutant was complemented by single-copy *CHM7* on a plasmid and also by the *CHM7ΔMIM* variant (Figure 10B). Thus, the MIM motif does not appear to be essential for Chm7 activity. The mCherry- and 3HA-tagged *CHM7* variants also complemented the temperature-sensitive defect (not shown).

To see whether the synthetic growth phenotype with *Δapq12* is specific for the *CHM7* deletion, double mutants were constructed for all ESCRT-III genes (Figure 11). A complication of this analysis is that deletions of the core ESCRT-III functions alone already display a temperature-sensitive phenotype at 37° (Weiss *et al.* 2008). For this reason, we also incubated the plates at a slightly less restrictive temperature (36°). The core ESCRT-III functions differed in the degree of temperature sensitivity. The temperature-sensitive phenotype was most severe with the *SNF7* and *VPS20* deletions,

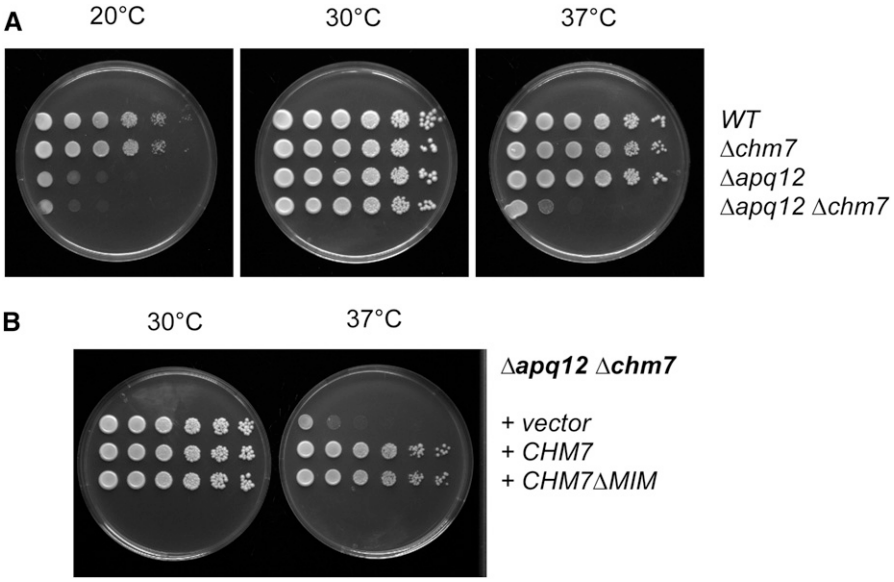


**Figure 10** Negative genetic interaction between *Δchm7* and *Δapq12*. Tenfold serial dilutions of fully grown overnight cultures were spotted onto YPD plates and incubated for 3 days at the temperatures indicated. (A) Strains (from top to bottom): JD52 (wild type), RKY2468 (*Δchm7*), RKY2685 (*Δapq12*), and RKY2693 (*Δapq12 Δchm7*). (B) RKY2693 (*Δapq12 Δchm7*) transformed with (from top to bottom) YCplac22 (vector), pRK1516 (*CHM7*), and pRK1511 (*CHM7ΔMIM1*).

which already barely grew at 36°, a temperature at which *VPS2*, *VPS24*, and *VTA1* deletions showed near-normal growth. From the group of ESCRT-III family members not considered to be part of ESCRT-III proper, only the *DID2* deletion displayed a temperature-sensitive phenotype at 37°, with normal growth at 36°. With the *Δapq12 ESCRT-III* double mutants, a synthetic growth phenotype was observed for *Δdid2*, *Δsnf7*, *Δvps2*, *Δvps24*, and, of course, *Δchm7*. The double mutants did not grow at all at 36°. For the *Δsnf7*, *Δvps2*, and *Δvps24* mutants, growth was already strongly compromised at 30°. No synthetic growth phenotype was observed for the *IST1*, *MOS10*, *VPS20*, and *VTA1* deletions. All mutants containing the *APQ12* deletion displayed a cold-sensitive phenotype at 20° similar to the *Δapq12* single mutant.

## Discussion

In this paper, we characterize for the first time the yeast ortholog of the human ESCRT-III-like protein CHMP7. We present evidence that Chm7 is not involved in endosomal sorting but rather seems to play a role at the ER membrane, possibly as part of an alternative ESCRT-III complex.

### *Does Chm7 play a role in the endocytic pathway?*

Horii *et al.* (2006) concluded that human CHMP7 functions in the endosomal sorting pathway. This notion rests on the finding that the fluorescent signal of endocytosed Rh-EGF persists longer in cells overexpressing GFP-CHMP7 than in untransfected cells. But it is not clear whether this effect is specific. The endosomal ESCRT-III complex and the CHMP7 complex seem to share common subunits; therefore, overexpression of CHMP7 could titrate away an essential ESCRT-III component, thus indirectly leading to a block in the endocytic pathway. It has been shown, for instance, that overexpression of CHMP4 leads to a relocalization of CHMP2B from the plasma membrane to internal CHMP4-containing structures, thus blocking CHMP2B function at the plasma membrane (Bodon *et al.* 2011).

Our findings argue against a contribution of yeast Chm7 to protein degradation via the endocytic pathway. We show that degradation of the endocytic cargo protein Ste6 and vacuolar sorting of CPS via the endocytic pathway are not affected by *CHM7* deletion. Also, in other respects, Chm7 does not behave like an endosomal ESCRT-III protein. It does not accumulate at the class E compartment on loss of Vps4 function, and its membrane association does not depend on Vps4.

The localization of fluorescent protein Chm7 fusions rather suggests that at least part of Chm7 could be associated with the ER. The sucrose density gradient profiles are in line with this notion. Also, a perinuclear localization of CHMP7 was reported by Horii *et al.* (2006).

Accumulation of the Chm7ΔMIM-mCherry fusion at the vacuolar membrane suggests that Chm7 function also could involve the vacuole. At present, it is unclear whether this distribution reflects a true function of Chm7 or is the result of an imbalance in the ESCRT system caused by the MIM deletion. MIM-MIT interactions could modulate the composition of ESCRT-III complexes. Lack of the MIM sequence of Chm7 could lead to the formation of an illegitimate mislocalized complex.

### *Is Chm7 part of an alternative ESCRT-III complex?*

Several of our observations support the notion that Chm7 is part of an alternative ESCRT-III complex. Most notably, the pattern of genetic interactions with the *APQ12* deletion is perfectly in line with the composition of the mammalian ESCRT-III complex involved in resealing of the nuclear envelope during mitosis. *APQ12* mutants are defective in NPC assembly and in mRNA export at low temperature (20°); at higher temperatures, these processes are normal (Scarcelli *et al.* 2007). We found that the *Δchm7*, *Δdid2*, *Δsnf7*, *Δvps2*,

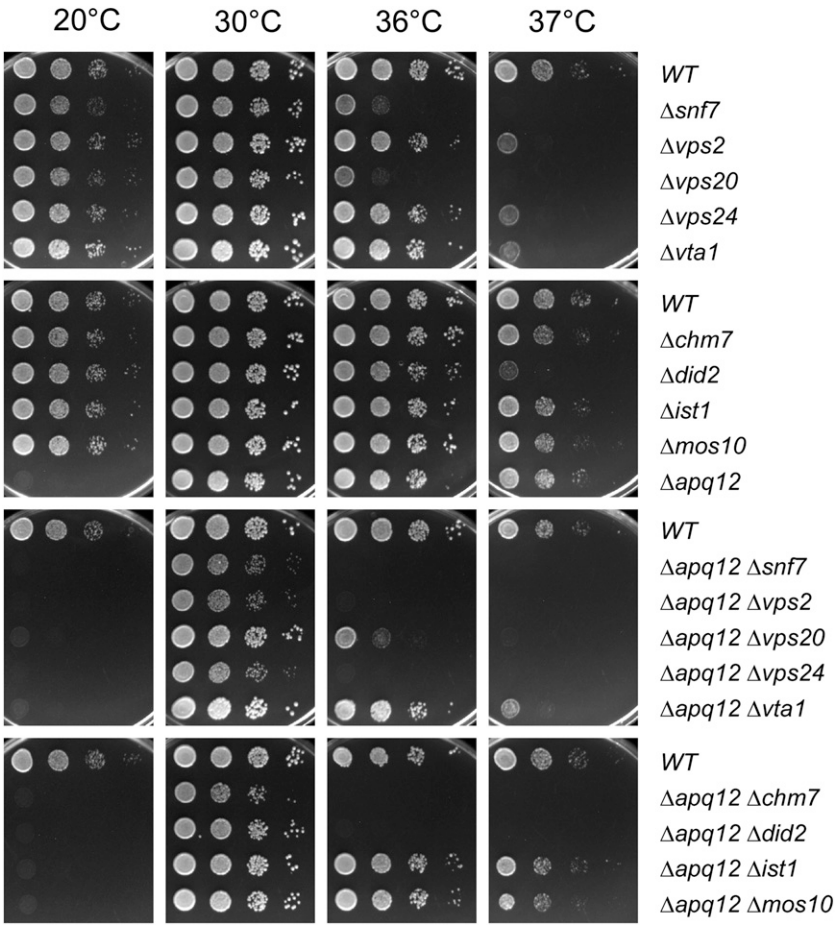


**Figure 11** Negative genetic interactions between ESCRT-III mutations and *Δapq12*. Tenfold serial dilutions of fully grown overnight cultures were spotted onto YPD plates and incubated for 2 days (30, 36, and 37°) or 3 days (20°). Strains (from top to bottom) are JD52, RKY1510, RKY1732, RKY1590, RKY1730, RKY2755, JD52, RKY2468, RKY1728, RKY2681, RKY1509, RKY2685, JD52, RKY2770, RKY2773, RKY2775, RKY2766, RKY2761, JD52, RKY2693, RKY2764, RKY2760, and RKY2759.

and *Δvps24* mutants display a synthetic growth defect with the *APQ12* deletion at elevated temperatures. These are exactly the yeast counterparts of the mammalian ESCRT-III proteins found in the CHMP7 complex involved in nuclear membrane resealing (CHMP7, CHMP1A/B, CHMP4A/B, CHMP2A, and CHMP3) (Vietri *et al.* 2015). Strikingly, lack of Vps20, which is a core component of the endosomal ESCRT-III complex, does not lead to a synthetic growth defect with *Δapq12*. Consistent with this finding, the mammalian counterpart CHMP6 was not detected in the CHMP7-containing ESCRT-III complex. This shows that the synthetic growth defects with the *APQ12* deletion are not simply a consequence of a defect in the endosomal ESCRT-III complex. Remarkably, the C-terminal part of Chm7 is most closely related to Vps20. Thus, it appears that Chm7 replaces Vps20 in the ER-localized ESCRT-III complex.

Further evidence for the existence of a Chm7-containing ESCRT-III complex comes from our two-hybrid analysis and from the localization of mCherry fusions. Two of the putative members of the Chm7 complex (Snf7 and Vps2) show a two-hybrid interaction with Chm7. Also, Vps2-mCherry (like Chm7-mCherry) accumulates in karmellae in *HMG1*-overexpressing cells, pointing to an ER localization of Vps2.

In all ESCRT-dependent processes studied so far, ESCRT-III is recruited to membranes by upstream regulators. In the case of the endosomal complex, ESCRT-III is recruited to membranes via an interaction between the ESCRT-II components Vps25 and Vps20 (Saksena *et al.* 2009). In addition, Vps20 has a general affinity for membranes owing to its N-terminal myristoylation (Ashrafi *et al.* 1998), which could explain the finding that Vps20-mCherry also could be detected in karmellae. We assume that the Vps25-like N-terminal domain of Chm7 targets the Chm7 complex to the ER membrane via an interaction with an as-yet-unknown upstream receptor. In line with this assumption, the mammalian complex involved in nuclear membrane resealing is targeted to the membrane by CHMP7 (Vietri *et al.* 2015).

What is unclear at the moment is the role of Ist1 for the Chm7 complex. Mammalian IST1 plays a central role for the complex involved in nuclear membrane resealing by recruiting the microtubule-severing ATPase spastin (Vietri *et al.* 2015). We also detected a two-hybrid interaction between Chm7 and Ist1, but we could not detect a synthetic growth phenotype with the *APQ12* deletion, which rather argues against a role of Ist1 in the yeast Chm7 complex. Also, quite unexpectedly, Ist1-mCherry localized to the nucleus. There is evidence that ESCRT-III proteins also have functions in the nucleus. Initially, CHMP1 was identified as a chromatin modifier (Stauffer *et al.* 2001), and evidence has been presented that yeast ESCRT-III proteins directly affect transcription in

the nucleus (Gaur *et al.* 2013). Interestingly, the CYCLoPs database reports a nuclear localization for Did2-GFP (Koh *et al.* 2015). This suggests that under certain conditions, ESCRT-III proteins may enter the nucleus.

*S. cerevisiae* has a closed mitosis, which is considered to be the most ancient form of mitosis. The spastin-recruiting subunit IST1 could have been acquired later during evolution by the CHMP7 complex at the transition from closed to open mitosis. Alternatively, Ist1 could be normally sequestered in the nucleus and could be released under special conditions to activate the cytoplasmic Chm7 complex.

Chm7 is an ancient protein already present in the "last common eukaryotic ancestor" (which did not have a nucleus) (Leung *et al.* 2008). Thus, the Chm7 complex could have a more fundamental function that remains to be elucidated. The *CHM7* deletion shows a synthetic growth defect with the *APQ12* deletion. This suggests that the Chm7 complex and Apq12 could have a common target. Evidence has been presented that *Δapq12* mutants are defective in the ability to adjust membrane lipid composition in response to low temperature, which could lead to the observed defects in NPC assembly and mRNA export (Scarcelli *et al.* 2007). The *CHM7* deletion, however, does not show a NPC assembly defect at any temperature (not shown). Still, it is conceivable that Chm7 also could be involved in adjusting the membrane composition to changes in environmental conditions. Alternatively, an altered membrane structure could lead to more severe stress at high temperature, and the Chm7 complex could be important for dealing with the consequences of stress.

To summarize, we have presented evidence that Chm7 does not function in the endosomal pathway but rather could play a role at the ER, presumably as part of a novel ESCRT-III complex. Although we did not succeed in presenting the final answer about the function of Chm7, we do think that our findings are highly relevant and are a good starting point to find out what Chm7 actually does.

## Acknowledgments

We thank Helge Paternoga for his valuable suggestions and his support. This work was supported by Deutsche Forschungsgemeinschaft (DFG) grant KO-963/5-2.

## Literature Cited

Ashrafi, K., T. A. Farazi, and J. I. Gordon, 1998 A role for *Saccharomyces cerevisiae* fatty acid activation protein 4 in regulating protein N-myristoylation during entry into stationary phase. J. Biol. Chem. 273: 25864–25874.

Babst, M., B. Wendland, E. J. Estepa, and S. D. Emr, 1998 The Vps4p AAA ATPase regulates membrane association of a Vps protein complex required for normal endosome function. EMBO J. 17: 2982–2993.

Babst, M., D. J. Katzmann, E. J. Estepa-Sabal, T. Meerloo, and S. D. Emr, 2002a ESCRT-III: an endosome-associated heterooligomeric protein complex required for MVB sorting. Dev. Cell 3: 271–282.

Babst, M., D. J. Katzmann, W. B. Snyder, B. Wendland, and S. D. Emr, 2002b Endosome-associated complex, ESCRT-II, recruits transport machinery for protein sorting at the multivesicular body. Dev. Cell 3: 283–289.

Bajorek, M., E. Morita, J. J. Skalicky, S. G. Morham, M. Babst *et al.*, 2009 Biochemical analyses of human IST1 and its function in cytokinesis. Mol. Biol. Cell 20: 1360–1373.

Baker, K. E., J. Coller, and R. Parker, 2004 The yeast Apq12 protein affects nucleocytoplasmic mRNA transport. RNA 10: 1352–1358.

Bodon, G., R. Chassefeyre, K. Pernet-Gallay, N. Martinelli, G. Effantin *et al.*, 2011 Charged multivesicular body protein 2B (CHMP2B) of the endosomal sorting complex required for transport-III (ESCRT-III) polymerizes into helical structures deforming the plasma membrane. J. Biol. Chem. 286: 40276–40286.

Cole, C., J. D. Barber, and G. J. Barton, 2008 The Jpred 3 secondary structure prediction server. Nucleic Acids Res. 36: W197–201.

Dimaano, C., C. B. Jones, A. Hanono, M. Curtiss, and M. Babst, 2008 Ist1 regulates Vps4 localization and assembly. Mol. Biol. Cell 19: 465–474.

Finn, R. D., A. Bateman, J. Clements, P. Coggill, R. Y. Eberhardt *et al.*, 2014 Pfam: the protein families database. Nucleic Acids Res. 42: D222–230.

Gaur, N. A., J. Hasek, D. G. Brickner, H. Qiu, F. Zhang *et al.*, 2013 Vps factors are required for efficient transcription elongation in budding yeast. Genetics 193: 829–851.

Ghazi-Tabatabai, S., S. Saksena, J. M. Short, A. V. Pobbati, D. B. Veprintsev *et al.*, 2008 Structure and disassembly of filaments formed by the ESCRT-III subunit Vps24. Structure 16: 1345–1356.

Hanson, P. I., R. Roth, Y. Lin, and J. E. Heuser, 2008 Plasma membrane deformation by circular arrays of ESCRT-III protein filaments. J. Cell Biol. 180: 389–402.

Henne, W. M., N. J. Buchkovich, Y. Zhao, and S. D. Emr, 2012 The endosomal sorting complex ESCRT-II mediates the assembly and architecture of ESCRT-III helices. Cell 151: 356–371.

Horii, M., H. Shibata, R. Kobayashi, K. Katoh, C. Yorikawa *et al.*, 2006 CHMP7, a novel ESCRT-III-related protein, associates with CHMP4b and functions in the endosomal sorting pathway. Biochem. J. 400: 23–32.

Howard, T. L., D. R. Stauffer, C. R. Degnin, and S. M. Hollenberg, 2001 CHMP1 functions as a member of a newly defined family of vesicle trafficking proteins. J. Cell Sci. 114: 2395–2404.

Hurley, J. H., and P. I. Hanson, 2010 Membrane budding and scission by the ESCRT machinery: it's all in the neck. Nat. Rev. Mol. Cell Biol. 11: 556–566.

James, P., J. Halladay, and E. A. Craig, 1996 Genomic libraries and a host strain designed for highly efficient two-hybrid selection in yeast. Genetics 144: 1425–1436.

Katzmann, D. J., M. Babst, and S. D. Emr, 2001 Ubiquitin-dependent sorting into the multivesicular body pathway requires the function of a conserved endosomal protein sorting complex, ESCRT-I. Cell 106: 145–155.

Kieffer, C., J. J. Skalicky, E. Morita, I. De Domenico, D. M. Ward *et al.*, 2008 Two distinct modes of ESCRT-III recognition are required for VPS4 functions in lysosomal protein targeting and HIV-1 budding. Dev. Cell 15: 62–73.

Koh, J. L., Y. T. Chong, H. Friesen, A. Moses, C. Boone *et al.*, 2015 CYCLoPs: a comprehensive database constructed from automated analysis of protein abundance and subcellular localization patterns in *Saccharomyces cerevisiae*. G3 5: 1223–1232.

Kölling, R., and C. P. Hollenberg, 1994 The ABC-transporter Ste6 accumulates in the plasma membrane in a ubiquitinated form in endocytosis mutants. EMBO J. 13: 3261–3271.

Kranz, A., A. Kinner, and R. Kölling, 2001 A family of small coiled-coil-forming proteins functioning at the late endosome in yeast. Mol. Biol. Cell 12: 711–723.

Lata, S., M. Roessle, J. Solomons, M. Jamin, H. G. Göttlinger *et al.*, 2008a Structural basis for autoinhibition of ESCRT-III CHMP3. J. Mol. Biol. 378: 818–827.

Lata, S., G. Schoehn, A. Jain, R. Pires, J. Piehler *et al.*, 2008b Helical structures of ESCRT-III are disassembled by VPS4. Science 321: 1354–1357.

Leung, K. F., J. B. Dacks, and M. C. Field, 2008 Evolution of the multivesicular body ESCRT machinery: retention across the eukaryotic lineage. Traffic 9: 1698–1716.

Longtine, M. S., A. McKenzie, D. J. Demarini, N. G. Shah, A. Wach *et al.*, 1998 Additional modules for versatile and economical PCR-based gene deletion and modification in *Saccharomyces cerevisiae*. Yeast 14: 953–961.

Morita, E., L. A. Colf, M. A. Karren, V. Sandrin, C. K. Rodesch *et al.*, 2010 Human ESCRT-III and VPS4 proteins are required for centrosome and spindle maintenance. Proc. Natl. Acad. Sci. USA 107: 12889–12894.

Muziol, T., E. Pineda-Molina, R. B. Ravelli, A. Zamborlini, Y. Usami *et al.*, 2006 Structural basis for budding by the ESCRT-III factor CHMP3. Dev. Cell 10: 821–830.

Nickerson, D. P., M. West, and G. Odorizzi, 2006 Did2 coordinates Vps4-mediated dissociation of ESCRT-III from endosomes. J. Cell Biol. 175: 715–720.

Obita, T., S. Saksena, S. Ghazi-Tabatabai, D. J. Gill, O. Perisic *et al.*, 2007 Structural basis for selective recognition of ESCRT-III by the AAA ATPase Vps4. Nature 449: 735–739.

Olmos, Y., L. Hodgson, J. Mantell, P. Verkade, and J. G. Carlton, 2015 ESCRT-III controls nuclear envelope reformation. Nature 522: 236–239.

Raymond, C. K., S. I. Howald, C. A. Vater, and T. H. Stevens, 1992 Morphological classification of the yeast vacuolar protein sorting mutants: evidence for a prevacuolar compartment in class E *vps* mutants. Mol. Biol. Cell 3: 1389–1402.

Remmert, M., A. Biegert, A. Hauser, and J. Soding, 2012 HHblits: lightning-fast iterative protein sequence searching by HMM-HMM alignment. Nat. Methods 9: 173–175.

Rieder, S. E., L. M. Banta, K. Köhrer, J. M. McCaffery, and S. D. Emr, 1996 Multilamellar endosome-like compartment accumulates in the yeast *vps28* vacuolar protein sorting mutant. Mol. Biol. Cell 7: 985–999.

Row, P. E., H. Liu, S. Hayes, R. Welchman, P. Charalabous *et al.*, 2007 The MIT domain of UBPY constitutes a CHMP binding and endosomal localization signal required for efficient epidermal growth factor receptor degradation. J. Biol. Chem. 282: 30929–30937.

Rue, S. M., S. Mattei, S. Saksena, and S. D. Emr, 2008 Novel Ist1-Did2 complex functions at a late step in multivesicular body sorting. Mol. Biol. Cell 19: 475–484.

Saksena, S., J. Wahlman, D. Teis, A. E. Johnson, and S. D. Emr, 2009 Functional reconstitution of ESCRT-III assembly and disassembly. Cell 136: 97–109.

Samson, R. Y., T. Obita, S. M. Freund, R. L. Williams, and S. D. Bell, 2008 A role for the ESCRT system in cell division in archaea. Science 322: 1710–1713.

Scarcelli, J. J., C. A. Hodge, and C. N. Cole, 2007 The yeast integral membrane protein Apq12 potentially links membrane dynamics to assembly of nuclear pore complexes. J. Cell Biol. 178: 799–812.

Skalicky, J. J., J. Arii, D. M. Wenzel, W. M. Stubblefield, A. Katsuyama *et al.*, 2012 Interactions of the human LIP5 regulatory protein with endosomal sorting complexes required for transport. J. Biol. Chem. 287: 43910–43926.

Stauffer, D. R., T. L. Howard, T. Nyun, and S. M. Hollenberg, 2001 CHMP1 is a novel nuclear matrix protein affecting chromatin structure and cell-cycle progression. J. Cell Sci. 114: 2383–2393.

Stuchell-Brereton, M. D., J. J. Skalicky, C. Kieffer, M. A. Karren, S. Ghaffarian *et al.*, 2007 ESCRT-III recognition by VPS4 ATPases. Nature 449: 740–744.

Teis, D., S. Saksena, and S. D. Emr, 2008 Ordered assembly of the ESCRT-III complex on endosomes is required to sequester cargo during MVB formation. Dev. Cell 15: 578–589.

Vietri, M., K. O. Schink, C. Campsteijn, C. S. Wegner, S. W. Schultz *et al.*, 2015 Spastin and ESCRT-III coordinate mitotic spindle disassembly and nuclear envelope sealing. Nature 522: 231–235.

Webster, B. M., P. Colombi, J. Jager, and C. P. Lusk, 2014 Surveillance of nuclear pore complex assembly by ESCRT-III/Vps4. Cell 159: 388–401.

Weiss, P., S. Huppert, and R. Kölling, 2008 ESCRT-III protein Snf7 mediates high-level expression of the *SUC2* gene via the Rim101 pathway. Eukaryot. Cell 7: 1888–1894.

Wollert, T., C. Wunder, J. Lippincott-Schwartz, and J. H. Hurley, 2009 Membrane scission by the ESCRT-III complex. Nature 458: 172–177.

Wright, R., M. Basson, L. D'Ari, and J. Rine, 1988 Increased amounts of HMG-CoA reductase induce "karmellae": a proliferation of stacked membrane pairs surrounding the yeast nucleus. J. Cell Biol. 107: 101–114.

*Communicating editor: M. D. Rose*